JOURNAL OF Materials CHEMISTRY

# Synthesis and electrochemical performance of dendrite-like nanosized SnSb alloy prepared by co-precipitation in alcohol solution at low temperature

**Hong Li, Guangyan Zhu, Xuejie Huang and Liquan Chen***

*Institute of Physics, Chinese Academy of Sciences, Beijing 100080, China*

***Received 10th August 1999, Accepted 8th December 1999***

A new reductive co-precipitation route to synthesize a pure phase nanosized β-SnSb alloy in alcohol solution at low temperature is reported. The morphology and particle size of the β-SnSb alloy are influenced by temperature, stirring and the solvent. The nanosized β-SnSb alloy prepared by this method shows good electrochemical performance as an anode material for lithium ion batteries. The β-SnSb alloy transforms gradually into multiphase $Li_3Sb$ and $Li_xSn$ with increased insertion of lithium ions. After extraction of the lithium ions, the original crystal structure of β-SnSb is restored, even after many cycles.

## Introduction

During the last decade, lithium ion batteries have achieved great success as a key component of portable electronic equipment essential for an information-rich, mobile society.[1] Consumers are still demanding batteries with larger energy densities and improvements will depend on the progress of exploring novel electrode materials. Compared with carbonaceous materials used as anode active materials in commercial lithium ion batteries, normally alloy-based anode materials have much higher specific capacities.[2–9] However, in most cases during the charge and discharge process, alloy-based anode materials exhibit large volume variations which gradually lead to the loss of electrical contact between the active alloy materials and the current collector, consequently, their reversible capacity fades with cycling.[7]

Recently, two strategies have been adopted to solve this problem. One is to use metal oxides as anode active materials, such as $SnO_2$, SnO and tin-based glasses.[10–14] During lithium ion insertion and extraction processes, nanosized Li–Sn alloys and amorphous $Li_2O$ are produced which are highly interspersed with each other *in situ*.[15] Thus, the volume variation of alloys caused by lithium insertion and extraction can be alleviated by an elastic environment. However, oxide-based anode materials exhibit rather large irreversible capacity loss during the first cycle. Such irreversible capacity loss in metal oxide anode materials is detrimental to the energy density of lithium ion batteries. A second method is to use superfine intermetallic alloys as anode materials. Such alloys show smaller absolute volume variation, stable dimensions and low capacity loss during cycling. Besenhard and co-workers have prepared the alloy $Sn_{0.78}Sb_{0.22}$ (0.56 Sn + 0.22 SnSb) with a particle size of *ca.* 300 nm by electroplating and by reductive precipitation.[7,16] This material shows better cycleability compared with pure metallic Sn. Moreover, owing to its large surface area and short ion diffusion length, an electrode composed of such nanosized particles shows good kinetic behavior,[17] a key factor for high power density batteries. Therefore, it is suggested that nanosized alloys are viable candidates to replace carbonaceous anode materials in lithium ion batteries.

Several methods have been developed to synthesize nanosized anode materials, such as high-energy ball milling,[18,19] electroplating[7,20] and reductive precipitation in aqueous solution.[16] However, it is not easy to obtain alloys of nanometer particle size and high purity by these methods.

Here, we report a new reductive precipitation route in alcohol solutions to synthesize nanosized pure phase β-SnSb alloy. The electrochemical performance of nano-SnSb used as an anode material for lithium ion batteries has also been investigated.

## Experimental

### Nano-SnSb alloy preparation

Nano-SnSb alloy was prepared by the reductive co-precipitation technique in ethane-1,2-diol solution in order to avoid hydrolysis. This method has been used to synthesize nanosized Co–Ni alloy,[21] Cu–Ni alloy[22] and III–V compounds.[23,24] For preparation of nano-SnSb alloy, $SbCl_3$ and $SnCl_2{\cdot}H_2O$ (99%, AR, Beijing Chemical Regent Company) were mixed together in a molar ratio of 5 : 4 and dissolved in ethane-1,2-diol to give a 0.5 M solution. The solution was cooled to 0.0–1.0 °C and Zn powder (99.9%, AR, Beijing Chemical Regent Company) (95% of stoichiometric amount) was added slowly under ultrasonication. Finally, after washing with ethanol and filtering off, the black product was dried under vacuum at 50 °C. Nano-SnSb alloy samples were also prepared in a similar manner in ethanol and glyceryl alcohol solutions. In addition, Some SnSb alloy samples were also synthesized in ethane-1,2-diol solution with or without ultrasonic stirring at room temperature, as well as by a solvothermal method at 130 °C, for comparison.

### Electrochemical experiment

The preparation of electrochemical cells was the same as described in our previous report.[15] The cell was composed of a metallic lithium foil as counter electrode, 1 M $LiPF_6$ in ethylene carbonate (EC)–diethyl carbonate (DEC) (1 : 1, v/v) as electrolyte, Celegard® 2300 as separator and nano-SnSb alloy as the working electrode. The working electrode was prepared by coating a binder-free slurry of nano-SnSb powder and cyclopentanone directly onto a surface-roughened copper foil (CARL Schlenk AG, Germany) in air. The film was dried at 80 °C for 8 h under vacuum, compressed under $1 \times 10^6$ Pa between two stainless steel plates and cut into pieces with areas of 0.8 $cm^2$. All cells were assembled in an argon-filled glove box. The cells were discharged and charged under a constant current density of 0.2 mA $cm^{-2}$ within a limited voltage range of 0.0–1.3 V. Cyclic voltammetry was performed on a CHI660 electrochemical workstation.

### Structure characterization

Structure characterization and *ex situ* XRD tests were carried out on a Rigaku B/max-2400 X-ray diffractometer using Cu radiation. The electrode films at different discharged states were fixed on a support and sealed in a glass container filled with Ar before the tests. The samples were exposed to air during XRD measurements which lasted for $\leqslant 8$ min. The morphology of nano-SnSb alloys was observed using a Hitachi S-4200 scanning electron microscope.

## Results and discussion

### Factors affecting particle size and morphology

The XRD patterns of SnSb alloys prepared in ethane-1,2-diol solution under different reaction conditions are shown in Fig. 1. The main diffraction peaks in each pattern are consistent with rhombohedral phase β-SnSb.[16,25] It can be seen from Fig. 1 that sample D prepared by a solvothermal method at 130 °C has the largest grain size. Sample A prepared at low temperature with ultrasonic treatment shows the smallest grain size and highest purity. The grain size of sample A is *ca.* 25 nm as estimated by the Scherrer formula. Impurities in sample B, C and D are remnant Sn or Sb. It is obvious that the temperature plays an important role in controlling the grain size of the particles. Ultrasonic treatment may aid in decreasing the inhomogeneity of the reaction caused by the higher viscosity of the solution at low temperature.

Besides temperature and ultrasonic stirring, it was found that the solvent has a significant influence on the particle size and the morphology of the SnSb alloy. Fig. 2 shows the SEM image of an SnSb alloy prepared in ethanol solution (sample E). Most of the particles were severely aggregated to form flocculent products and only a few showed a feather-like appearance as shown in the center region of Fig. 2. Two main branches and many small 'fine hair' structures can be seen. The length of the main branch is about 3 μm whereas the 'fine hair' structures range from 100 to 300 nm.

The morphology of SnSb alloy prepared in ethane-1,2-diol solution (sample A) is very different from that of sample E. Most of the particles have a dendritic appearance as shown in Fig. 3(a). In a magnified (zoom) image, a typical pine-like structure can be seen clearly in the left portion in Fig. 3(b). 'Leaves' of different lengths and widths connect along the main branch. The length of each 'leaf' ranges from 700 to 100 nm with widths from 200 to 70 nm. Moreover, each leaf shows fine structure. On each leaf, there is a main branch composed of many small quadrate joints. Beside the main branch, many loose-leaf like structures can be seen. The size of the larger joints is about $90 \times 45$ nm while the thickness of the side 'leaves' is $<20$ nm. In addition, some aggregates composed of nanosized particles are apparent from this image. At the right-hand corner in Fig. 3(b), a group of fork-like particles of width $<100$ nm can be observed.

Fig. 4(a) shows the image of SnSb alloy prepared in glyceryl alcohol solution (sample F). It can be seen that virtually each particle has a pine-leaf-like appearance. In a zoom image, a fish-bone-like structure can be seen clearly in Fig. 4(b). The main branch is composed of many triangular joints of $<60$ nm. The appearance of the branches is different from that of sample A. The branches are composed of many quadrate joints instead of an 'axial-leaf' structure. The size of these joints is $<60$ nm.

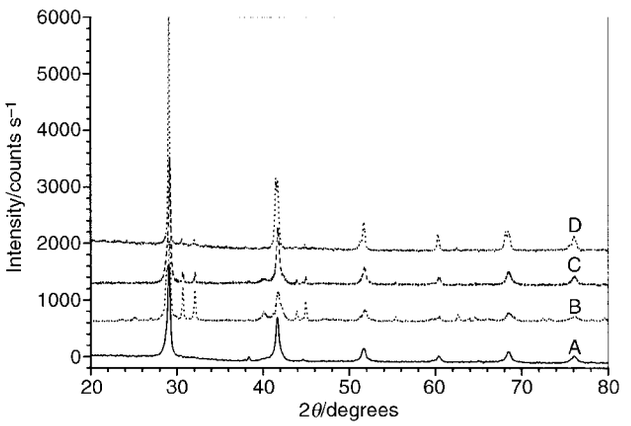


**Fig. 1** XRD patterns of SnSb alloys prepared by reductive co-precipitation in ethane-1,2,-diol solution. (A) 0 °C, with ultrasonic treatment (sample A), (B) room temperature, without ultrasonic treatment (sample B), (C) room temperature, with ultrasonic treatment (sample C) and (D) 130 °C solvothermal synthesis.


**Fig. 2** SEM image of SnSb alloy prepared by reductive co-precipitation in ethanol solution at 0.0–1.0 °C with ultrasonic treatment (sample E). A feather-like particle with two branches can be seen in the center region.

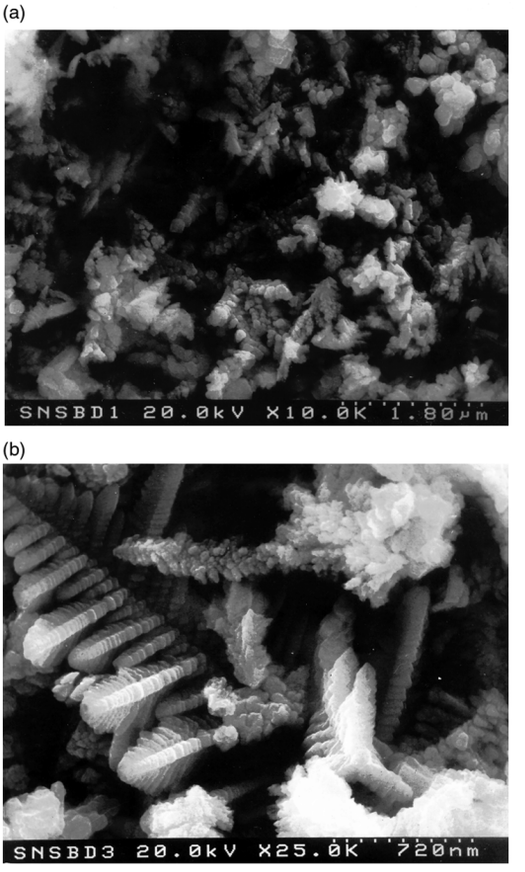


**Fig. 3** The SEM images of SnSb alloy prepared by reductive co-precipitation in ethane-1,2-diol solution at 0.0–1.0 °C under ultrasonic treatment (sample A). (a) Low magnification, many dendritic particles can be seen. (b) Local zoom, pine- and fork-like structures can be seen.

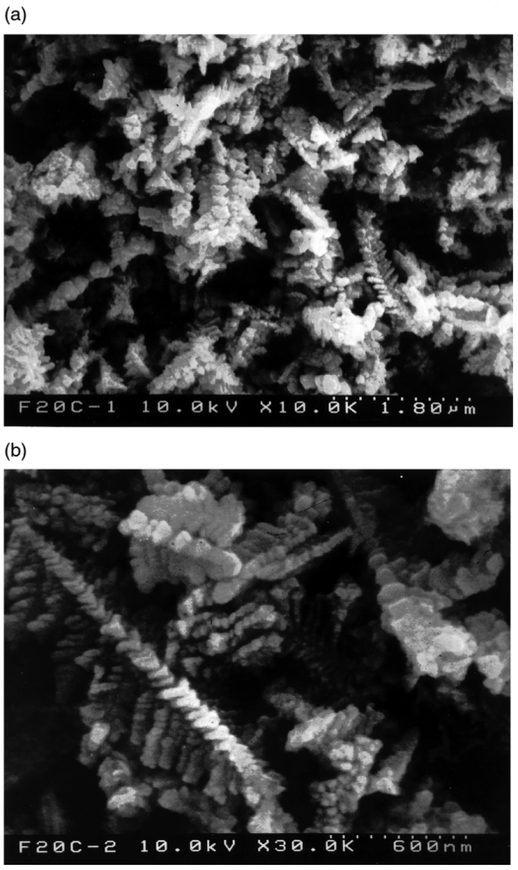


**Fig. 4** SEM images of SnSb alloy prepared by reductive co-precipitation in glyceryl alcohol solution at 0.0–1.0 °C under ultrasonic treatment (sample F). (a) Pine-leaf-like nanosized SnSb alloy. (b) Local zoom image of 'leaf-like' structure.

In conclusion, the dendritic morphology of SnSb alloy is very well developed in glyceryl alcohol solution with the sizes of the joints in the particle being smallest. Since the viscosity of the glyceryl alcohol solution is the highest among the three reaction systems investigated the diffusion rate of $Sn^{2+}$ and $Sb^{3+}$ should be the lowest and thus, local inhomogeneity is more significant. This factor may promote the formation of dendritic structure, while SnSb alloy particles in ethanol solution may grow homogeneously to avoid dendritic structure. Further investigation is required to delineate the influence of the solvent on the particle morphology.

## Improvement of electrochemical performance

Discharge/charge curves of a lithium cell: nano-SnSb|1 M $LiPF_6$, EC–DEC (1 : 1, v/v)|Li are shown in Fig. 5. In order to avoid interference from the binder and the conductive additive, the working electrode is composed of pure nano-SnSb powder. Thus, the voltage profile indicates directly the electrochemical performance of nano-SnSb. It can be divided into three regions at the first discharge as indicated in Fig. 5. Region I is a slope in the range 1.3–0.8 V which disappears in the later cycles. Based on our previous studies on $Sb_2O_3$ anodes,[9] this region can be attributed to a decomposition reaction caused by a surface oxide layer on nano-SnSb. Region II is a voltage plateau at 0.8 V. A corresponding charging plateau can be also seen at 1.1 V. According to our previous result,[26] this voltage region should be related to the reaction of Li–Sb alloy. Region III is a slope consisting of several plateaus in the range 0.7–0.0 V. The shape of the voltage curve is similar with that of Sn or Sn-based oxide anodes.[11,15,27] The multi-step Li–Sn alloy reactions are completed in this voltage range. The profile in region II and III

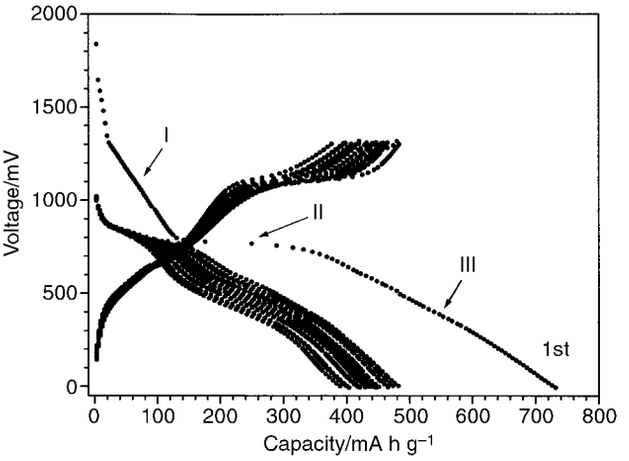


**Fig. 5** Discharge–charge curves of a nano-SnSb anode in a lithium cell: nano-SnSb (sample A)|1 M $LiPF_6$, EC–DEC (1 : 1, v/v)|Li. Current density = 0.2 mA cm$^{-2}$. Roman numbers indicate the three reaction regions: surface oxide decomposition (I), Li–Sb alloy reaction (II) and Li–Sn alloy reaction (III).

is more smooth than that reported by Besenhard *et al.*[7] for $Sn_{0.78}Sb_{0.22}$ and may be related to the smaller particle size.

The electrode reaction processes can be distinguished more clearly in the cyclic voltammogram as shown in Fig. 6. Several reduction peaks can be observed in the first cycle corresponding to the voltage plateaus in Fig. 5. Previously, we have investigated the cyclic voltammogram of $Sb_2O_3$ and SnO.[9] Two pairs of reversible redox peaks for the $Sb_2O_3$ anode which have been recognized as $Li_2Sb$ and $Li_3Sb$ alloy reactions were found in the same potential range as the peaks B and B′ in Fig. 6. Six pairs of redox peaks for an SnO anode attributed to Li–Sn alloys were observed in a similar potential range encompassed by C and C′ in Fig. 6. Therefore, possible electrochemical reactions of nanosized SnSb with Li may be described as below:

$$x\mathrm{Li}^+ + \mathrm{e}^- + (\mathrm{Sb_2O_3},\ \mathrm{SnO})_{\mathrm{surface}} \rightarrow \mathrm{Li_2O} + (\mathrm{Sb},\ \mathrm{Sn})_{\mathrm{surface}} \quad (1)$$

$$y\mathrm{Li}^+ + \mathrm{e}^- + \mathrm{SnSb} + (\mathrm{Sb},\ \mathrm{Sn})_{\mathrm{surface}} \rightarrow \mathrm{Li}_y\mathrm{Sb} + \mathrm{Sn} \quad (y<3) \quad (2)$$

$$z\mathrm{Li}^+ + \mathrm{e}^- + \mathrm{Sn} \rightarrow \mathrm{Li}_z\mathrm{Sn} \quad (z<4) \quad (3)$$

An electrolyte decomposition reaction might also occur, since a passivating film has been observed on the surface of SnO and Sn anodes,[15,28,29] and may overlap with peaks A and B in the first cycle. Indeed the current density of the redox peaks B and B′ (Fig. 6) decreases significantly in the second cycle which is

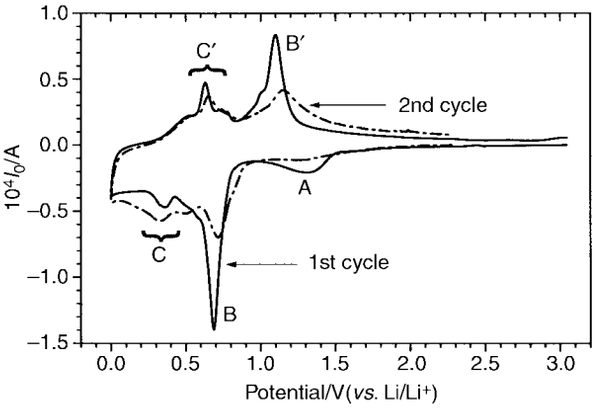


**Fig. 6** Cyclic voltammogram of a nano-SnSb anode in a lithium cell: sample A|1 M $LiPF_6$, EC–DEC (1 : 1, v/v)|Li/Li. Scanning rate = 0.02 mV s$^{-1}$. The area of the working electrode is 0.64 cm$^2$. The reduction peaks in the first cycle denoted by A, B and C correspond to the voltage plateaus I, II, III, respectively, in Fig. 5.

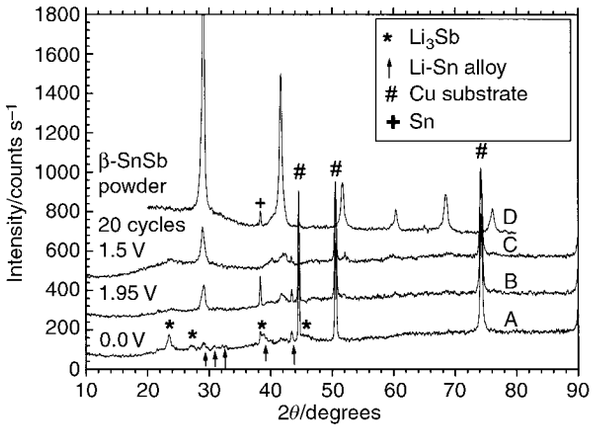


**Fig. 7** *Ex situ* XRD patterns of nano-SnSb anodes at different discharged states in lithium cells of Fig. 5 and 6. (A) Discharged to 0.0 V *vs.* $Li/Li^+$ at the first cycle, (B) after step A, then charged to 1.95 V *vs.* $Li/Li^+$, (C) after 20 discharge–charge cycles, stopped at 1.5 V *vs.* $Li/Li^+$, (D) original nano-SnSb powder (sample A).

consistent with the results of Fig. 5. This phenomenon implies that the reaction of Sb with lithium leads to a larger irreversible capacity loss than the reaction of Sn with Li and may be attributed to the stronger affinity between Sb and Li.

Compared with our previous studies on Sn and nano-Sb anode materials,[26,30] the cyclability of nano-SnSb is obviously better than for individual Sn and Sb anodes. This may be related to the special microstructure of the SnSb alloy. In addition, both Sn and Sb in the SnSb alloy are active and inserted lithium ions will react with both elements. Besenhard *et al.*[7] proposed that reacted SnSb may be embedded in an unreacted soft and ductile Sn matrix (in their case, mole ratio of Sn : SnSb in the precursor = 0.78 : 0.22). In our case, the precursor is pure phase SnSb alloy and is more suitable for studying the reaction mechanism.

Fig. 7 shows *ex situ* XRD patterns of nano-SnSb at different discharged states. It can be seen that the SnSb anode in the discharged state during the first cycle was essentially transformed into $Li_3Sb$ and Li–Sn alloys as shown in Fig. 7(A). In the charged state, by comparison with the original structure as shown in Fig. 7(D), the crystal structure of β-SnSb is restored even after 20 cycles as shown in Fig. 7(B) and (C). β-SnSb has a rhombohedral phase structure in which Sn and Sb atoms occupy periodic lattice planes alternately in the *c* direction. According to the discharge/charge curves and cyclic voltammogram as shown in Fig. 5 and 6, respectively, inserted lithium ions react first with Sb atoms to form $Li_3Sb$, and then react further with Sn atoms to form Li–Sn alloys. Since $Li_3Sb$ and $Li_xSn$ phases can be seen clearly in the deeply discharged state in Fig. 7, phase separation clearly occurs. It is thus concluded that during insertion of lithium ions, Sb and Sn atoms leave their original lattice sites and concentrate locally. After lithium ions have been extracted, such separated Sn and Sb atoms rebond to restore the original β-SnSb alloy structure. This indicates that Sn and Sb atoms have a strong affinity for each other and thus the structure of β-SnSb alloy is stable. Such self-restoration is beneficial for the cyclic performance of the nano-SnSb anode. Furthermore, dramatic crystal structure variation can be performed reversibly many times at room temperature implying a very strong cooperation process and fast diffusion rate of Sn, Sb and Li atoms in the matrix. Further investigations are required to more fully determine the structure evolution mechanism.

## Conclusions

This preliminary work indicates that the technique of reductive co-precipitation in organic solvents at low temperature is an effective method to prepare nanosized pure phase β-SnSb alloy. The morphology and particle size can be controlled by variation of solvent, temperature and stirring conditions. The resulting nanosized β-SnSb alloy shows a good electrochemical performance. During discharge processes, the original β-SnSb phase is transformed into a multiphase composed of $Li_3Sb$ and $Li_xSn$, while after lithium ions have been extracted, the original crystal structure of β-SnSb alloy is restored.

## Acknowledgements

This research is supported by Ford-NSFC Foundation (contract No. 9712304), NSFC (contract No. 59972041 and 19774022) and National 863 Key Program (contract No. 715-004-0280).

## References

1 J. M. Tarascon, in *Extended abstracts for 12th International Conference on Solid State Ionics*, Halkidiki, Greece, June 6, 1999, PL-01, p. 9.
2 B. Rao, R. Francis and H. W. Christopher, *J. Electrochem. Soc.*, 1977, **124**, 1490.
3 M. Garreau, J. Thevenin and M. Fekir, *J. Power Sources*, 1983, **9**, 235.
4 J. Wang, P. King and R. A. Huggins, *Solid State Ionics*, 1986, **20**, 185.
5 J. Wang, I. D. Raistrick and R. A. Huggins, *J. Electrochem. Soc.*, 1986, **133**, 457.
6 A. A. Anani, S. C. Baker and R. A. Huggins, *J. Electrochem. Soc.*, 1987, **134**, 3098.
7 J. O. Besenhard, J. Yang and M. Winter, *J. Power Sources*, 1997, **68**, 87.
8 R. A. Huggins, *Solid State Ionics*, 1998, **113**, 57.
9 H. Li, X. J. Huang and L. Q. Chen, *Solid State Ionics*, 1999, **123**, 189.
10 Y. Idota, T. Kubota, A. Matsufuji, Y. Maekawa and T. Miyasaka, *Science*, 1997, **276**, 1395.
11 I. A. Courtney and J. R. Dahn, *J. Electrochem. Soc.*, 1997, **144**, 2045.
12 W. F. Liu, X. J. Huang, Z. X. Wang, H. Li and L. Q. Chen, *J. Electrochem. Soc.*, 1998, **145**, 59.
13 I. A. Courtney and J. R. Dahn, *J. Electrochem. Soc.*, 1997, **144**, 2943.
14 T. Brousse, R. Retoux, U. Herterich and D. M. Schleich, *J. Electrochem. Soc.*, 1998, **145**, 1.
15 H. Li, X. J. Huang and L. Q. Chen, *Electrochem. Solid-State Lett.*, 1998, **1**, 241.
16 J. Yang, M. Wachtler, M. Winters and J. O. Besenhard, *Electrochem. Solid-State Lett.*, 1999, **2**, 161.
17 H. Li, X. J. Huang, L. Q. Chen, Z. G. Wu and Y. Liang, *Electrochem. Solid-State Lett.*, 1999, **2**, 547.
18 O. Mao, *Electrochem. Solid-State Lett.*, 1999, **2**, 3.
19 O. Mao, R. A. Dunlap, I. A. Courtney and J. R. Dahn, *J. Electrochem. Soc.*, 1998, **145**, 4195.
20 J. Yang, M. Winter and J. O. Besenhard, *Solid State Ionics*, 1996, **90**, 281.
21 G. Chow, L. Kurihara and K. Kemner, *J. Mater. Res.*, 1995, **10**, 1546.
22 Y. D. Li, Ph.D. Thesis, Chinese Science and Technology University, 1998.
23 Y. Xie and Y. Qian, *Science*, 1996, **272**, 1926.
24 Y. D. Li, X. Duan and Y. Qian, *J. Am. Chem. Soc.*, 1997, **119**, 7867.
25 β-SnSb, JCPDS, 33-0118.
26 H. Li, unpublished data.
27 J. Wang, I. D. Raistrick and R. A. Huggins, *J. Electrochem. Soc.*, 1986, **133**, 457.
28 H. Li, X. J. Huang and L. Q. Chen, *J. Power Sources*, 1999, **81–82**, 340.
29 A. V. Churikov, E. S. Nimon and A. L. Lvov, *Electrochim. Acta*, 1997, **42**, 179.
30 H. Li, X. J. Huang and L. Q. Chen, *J. Power Sources*, 1999, **81–82**, 335.

*Paper a906491e*